

SUPPORTING INFORMATION FOR THE MANUSCRIPT:

Fueling biomass-degrading oxidative enzymes by light-driven water oxidation

Bastien Bissaro^{a,b*}, Zarah Forsberg^b, Yan Ni^c, Frank Hollmann^c, Gustav Vaaje-Kolstad^b, and
Vincent G.H. Eijssink^b

a. INRA, UMR792, Ingénierie des Systèmes Biologiques et des Procédés, F-31400 Toulouse, France

b. Department of Chemistry, Biotechnology and Food Science, Norwegian University of
Life Sciences (NMBU), P.O. Box 5003, N-1432 Aas, Norway

c. Department of Biotechnology, Delft University of Technology, Julianalaan 136, Delft 2628BL, The Netherlands.

*Corresponding author:

bastien.bissaro@nmbu.no

SI Appendix Table of content

Supplementary Experimental. Fluorescence data analysis

Figure S1. Proof-of-concept for photobiocatalytic oxidation of cellulose.

Figure S2. Control reactions to check for occurrence of copper-catalyzed Fenton-type chemistry.

Figure S3. A substrate- and LPMO family-independent photobiocatalytic system.

Figure S4. Harvesting sunlight energy.

Figure S5. Impact of putative alternative electron donors (methanol or formate) on the photobiocatalytic oxidation of cellulose by ScLPMO10C.

Figure S6. The effect of phosphate on the photobiocatalytic system.

Figure S7. Role of polyprotic acids in the oxidation of Avicel by ScLPMO10C/V-TiO₂ upon visible light exposure.

Figure S8. Impact of H₂O₂ on ScLPMO10C activity.

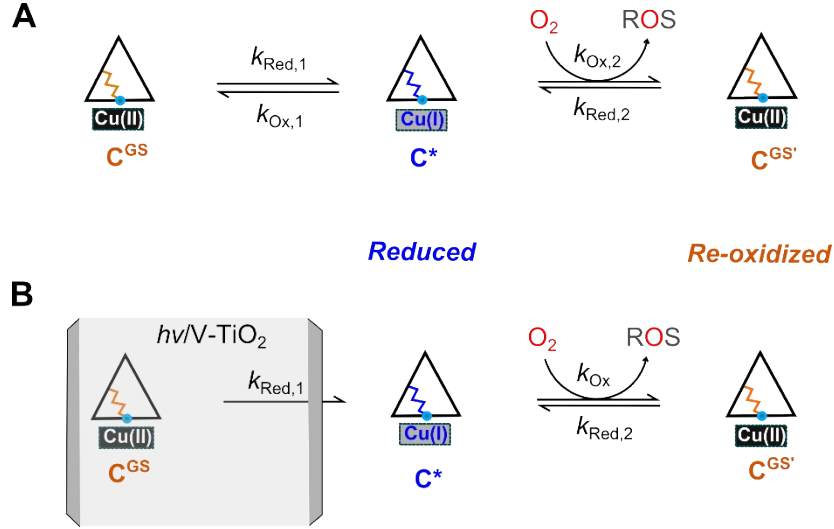
Figure S9. Schematic representation of the possible fate of electrons generated by light-driven water oxidation.

Figure S10. Redox state-dependent fluorescence properties of ScLPMO10C.

Figure S11. Probing LPMO redox intermediate formation for different redox systems by fluorescence spectrophotometry.

Figure S12. Shedding light on the spatio-temporal origin of electrons in the catalytic mechanism of LPMOs using the photobiocatalytic system.

Fluorescence data analysis. When $h\nu/V\text{-TiO}_2$ is employed as a reducing system to activate the enzyme, it can be removed from the solution before monitoring fluorescence intensity. Since the electron source is removed the subsequent decay reaction for the intermediate (C^*) is substantially simplified as illustrated below:



Legend : A simplified model of reduction and oxygen-mediated re-oxidation of the LPMO copper center. (A) The LPMO-Cu(II) (ground state complex, C^{GS}) receives electrons from a reducing agent (e.g. ascorbic acid) leading to a reduced complex (C^* species). The C^* species reacts then with oxygen, leading to an oxidized intermediate LPMO-Cu(II)- $O_2^{\bullet-}$, which in the absence of substrate leads to generation of reactive oxygen species (notably H_2O_2), ultimately restoring the ground state. The re-oxidized Cu(II) state can therefore be found in the free state of the LPMO (C^{GS} species) or in one of the oxygen-bound intermediates. The re-oxidized forms are designated as $C^{GS'}$. **(B)** When using $h\nu/V\text{-TiO}_2$ as a generator of reducing power, the latter can be removed (grey shading) from the reaction medium before fluorescence monitoring which simplifies (in terms of parallel reactions occurring) the observation of subsequent decay of the C^* species.

From the reaction scheme in panel B (pre-activation by $h\nu/V\text{-TiO}_2$), the following equation can be derived:

$$\frac{d[C^*]}{dt} = -k_{ox}[C^*].[O_2] + k_{Red,2}[C^{GS'}].[ROS]$$

which may be simplified to:


$$\frac{d[C^*]}{dt} = -c.k_{ox}[C^*]$$

by:

(1) Assuming that the reaction is irreversible, meaning that $k_{Red,2} \ll k_{ox}$

and

- (2) Taking into account that $[O_2]$ is saturating and a constant, $c. [O_2] = 258 \mu M$ at $25^\circ C$ which is much larger than $[C^*]$ (< 2 to $14 \mu M$ depending on experiments); stirring ensures that diffusion of oxygen from the head space is replacing consumed oxygen in the solution.

After reduction of C_0 to C^* , the concentration of C^* at time t can be described by a standard single exponential decay equation (Equation 1): 

$$\int_{C_1}^{C^*} \frac{d[C^*]}{[C^*]} = \int_{t_1}^t -c.k_{ox}.dt$$

$$[\ln]_{C_1}^{C^*}([C^*]) = -c.k_{ox}.(t - t_1)$$

$$\ln\left(\frac{[C^*]}{[C_1]}\right) = -c.k_{ox}.(t - t_1)$$

$$[C^*] = [C_1].e^{-c.k_{ox}.(t - t_1)} \quad \text{Equation (1)}$$

Where t_1 represents the time at which the decay starts and $C_1 = C^*_{t=t_1}$ (i.e. when observed fluorescence is maximum, F_1 in **Fig. 5A**).

To relate the protein concentration to the measured fluorescence it is reasonable to assume that the protein concentration is proportional to fluorescence intensities both in the oxidized (GS') and in the reduced state ($*$), which translates in:

$$F^{GS'} = f^{GS'} . C^{GS'}$$

$$F^* = f^* . C^*$$

With f being the fluorescence coefficient, which is different for the two states, i.e. the Cu(II) state ($f^{GS'}$) and the Cu(I) (f^*) state.

The measured fluorescence (F) corresponds to the added fluorescence of both species, oxidized or reduced.

Hence,

$$F = F^{GS'} + F^*$$

$$F = f^{GS'} . C^{GS'} + f^* . C^* \quad \text{Equation (2)}$$

The total concentration of enzyme is equal to the sum of both entities $C^{tot} = C^{GS}_{t=0} = C^{GS'} + C^*$

So equation (2) leads to : $F = f^{GS'}.(C^{tot} - C^*) + f^*.C^*$

$$\text{Rewritten as } F = f^{GS'} . C^{tot} + (f^* - f^{GS'}) . C^* \quad \text{Equation (3)}$$

It is assumed that the enzyme is fully oxidized at $t = 0$, therefore the fluorescence $F_0 = f^{GS} \cdot C^{tot} = f^{GS'} \cdot C^{tot}$

(Here the approximation $f^{GS} = f^{GS'}$ is made)

Which combined with Equation (3) leads to $F - F_0 = (f^* - f^{GS'}) \cdot C^*$

or

$$(F - F_0)/F_0 = \left(\frac{f^* - f^{GS'}}{f^{GS'}} \right) \cdot \frac{C^*}{C^{tot}} \quad \text{Equation (4)}$$

At $t = t_1$, $C^* = C_1$ and $F = F_1 = F_{max}$

$$\text{So Equation (4) gives } (F_1 - F_0)/F_0 = \left(\frac{f^* - f^{GS'}}{f^{GS'}} \right) \cdot \frac{C_1}{C^{tot}}$$

Combined with **Equation (1)** one can obtain:

$$\frac{[C^*]}{[C_1]} = e^{-c.k_{ox}(t-t_1)} = \frac{C^{tot} \cdot \left(\frac{(F - F_0)/F_0}{\left(\frac{f^* - f^{GS'}}{f^{GS'}} \right)} \right)}{C^{tot} \cdot \left(\frac{(F_1 - F_0)/F_0}{\left(\frac{f^* - f^{GS'}}{f^{GS'}} \right)} \right)}$$

Simplified to:

$$F = (F_1 - F_0) \cdot e^{-c.k_{ox}(t-t_1)} + F_0 \quad \text{Equation (5)}$$

Notably, the physical phenomenon of intrinsic fluorescence decay usually has a timescale in the range of 0.5-10 ns depending on interactions and polarity of the environment, which is far from the timescale of the decay monitored here (tenths of minutes). Thus, the change in fluorescence signals observed here relates to enzymatic behaviour rather than to a physical phenomenon.

The half-life of the intermediate can be determined by **Equation (6)**, which is derived from **Equation (1)**

$$\text{by defining } t = t_{1/2} \text{ when } C^* = \frac{C_1}{2}$$

$$t_{1/2} = \frac{\ln(2)}{c.k_{ox}} + t_1 \quad \text{Equation (6)}$$

The decay of ScLPMO10C after reduction by $h\nu/V\text{-TiO}_2$ and separation from the reductant was fitted by non-linear regression (least-squares method) to **Equation (5)**, rewritten as a single-exponential decay model, which yielded the following parameters:

$$\frac{(F - F_0)}{(F_1 - F_0)} = e^{-c.k_{ox}(t-t_1)} = e^{-k_{app}(t-t_1)}$$

$$k_{ox} = 86.7 \text{ M}^{-1}.\text{min}^{-1} \text{ or } k_{app} = 0.0224 \text{ min}^{-1} \text{ (with } c = [\text{O}_2] = 2.58 \cdot 10^{-4} \text{ M)}$$

k_{app} is the apparent turnover number for decay of reduced LPMO in the absence of substrate. The half-life of the reaction, derived from **Equation (6)**, is 36.1 min.

Fluorescence data displayed in **Fig. 5B** are represented as $(F-F_0)/F_0$ to show the relative increase in fluorescence compared to the ground state level.

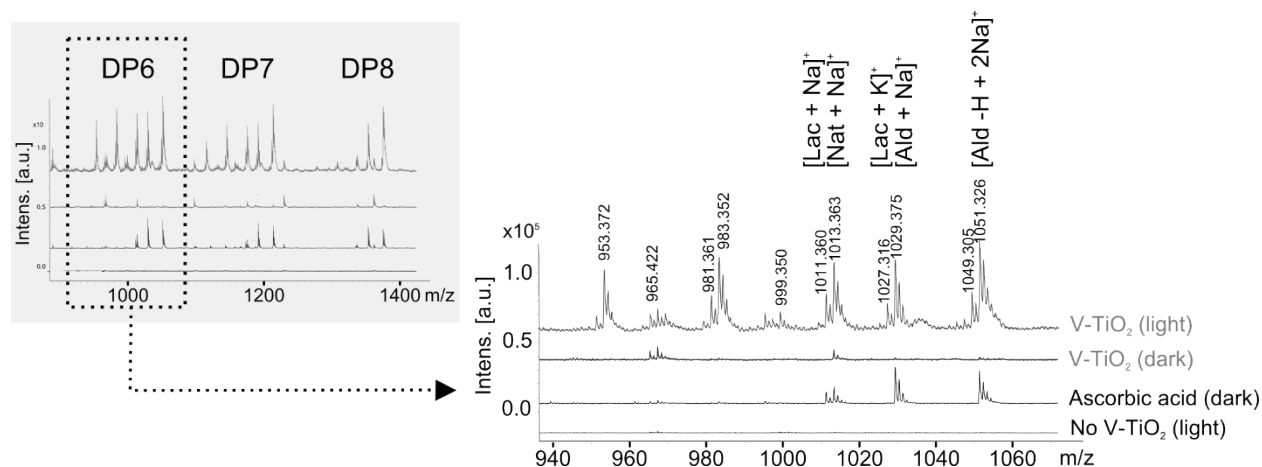


Figure S1. Proof-of-concept for photobiocatalytic oxidation of cellulose. MALDI-TOF MS analysis of products generated from Avicel (10 g.L⁻¹) by ScLPMO10C (0.9 μM) after 22 h of incubation. Reactions were carried out in sodium phosphate buffer (50 mM, pH 6.0) at 40 °C, under magnetic stirring. Reaction conditions varied in terms of exposure to visible light ($I = 10\%$; I_{max} , approx. 16.6 W.cm²), the presence of ascorbic acid (1 mM) and the presence of V-TiO₂ (10 g.L⁻¹). The figure shows the DP6 – DP8 region (grey insert) as well as an enlargement of the DP6 region. The abbreviations indicate sodium or potassium adducts of native (Nat) or oxidized oligosaccharide in the lactone form (Lac) or the aldonic acid form (Ald). Note that the 1051 signal is diagnostic of aldonic acids, since the introduced carboxyl group is needed to obtain double sodium adducts. Please note that the MALDI-TOF MS analysis only provides a qualitative evaluation, and is not quantitative.

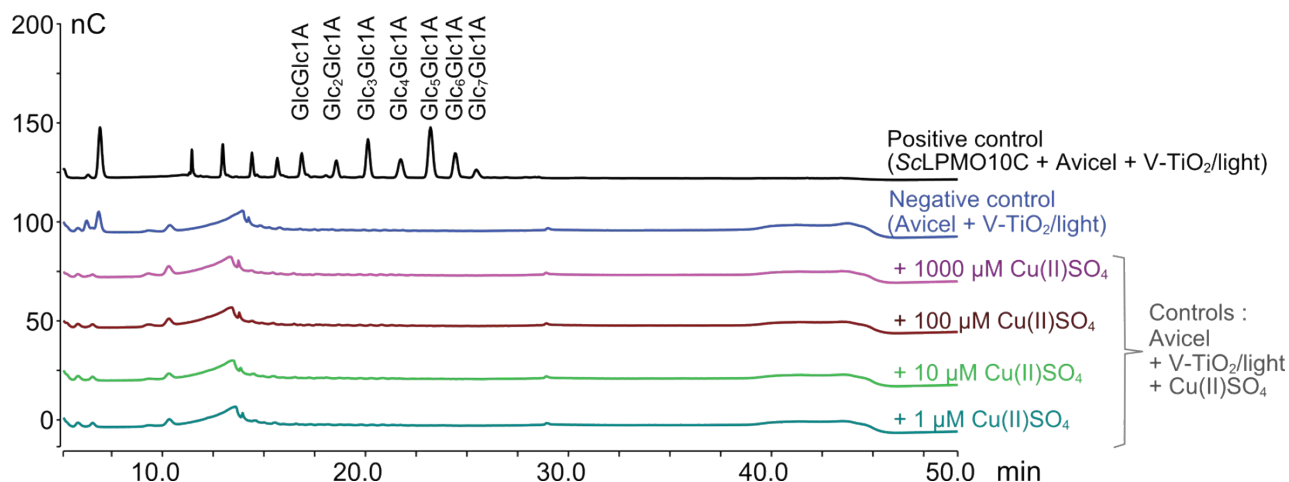


Figure S2. Control reactions to check for the occurrence of copper-catalyzed Fenton-type chemistry.

The enzyme, ScLPMO10C, was replaced by different concentrations of Cu(II)SO₄ (0-1000 μM) whereas the positive control contained 1 μM of ScLPMO10C. All reactions were carried out in sodium phosphate buffer (50 mM, pH 6.0) and incubated for 4 h at 40 °C, in glass vials under magnetic stirring, exposed to a light intensity of 25% of maximum intensity (approx. 42 W.cm⁻²). All reaction mixtures contained Avicel (10 g.L⁻¹) and V-TiO₂ (5 g.L⁻¹). Glc1A, aldonic acid of glucose.

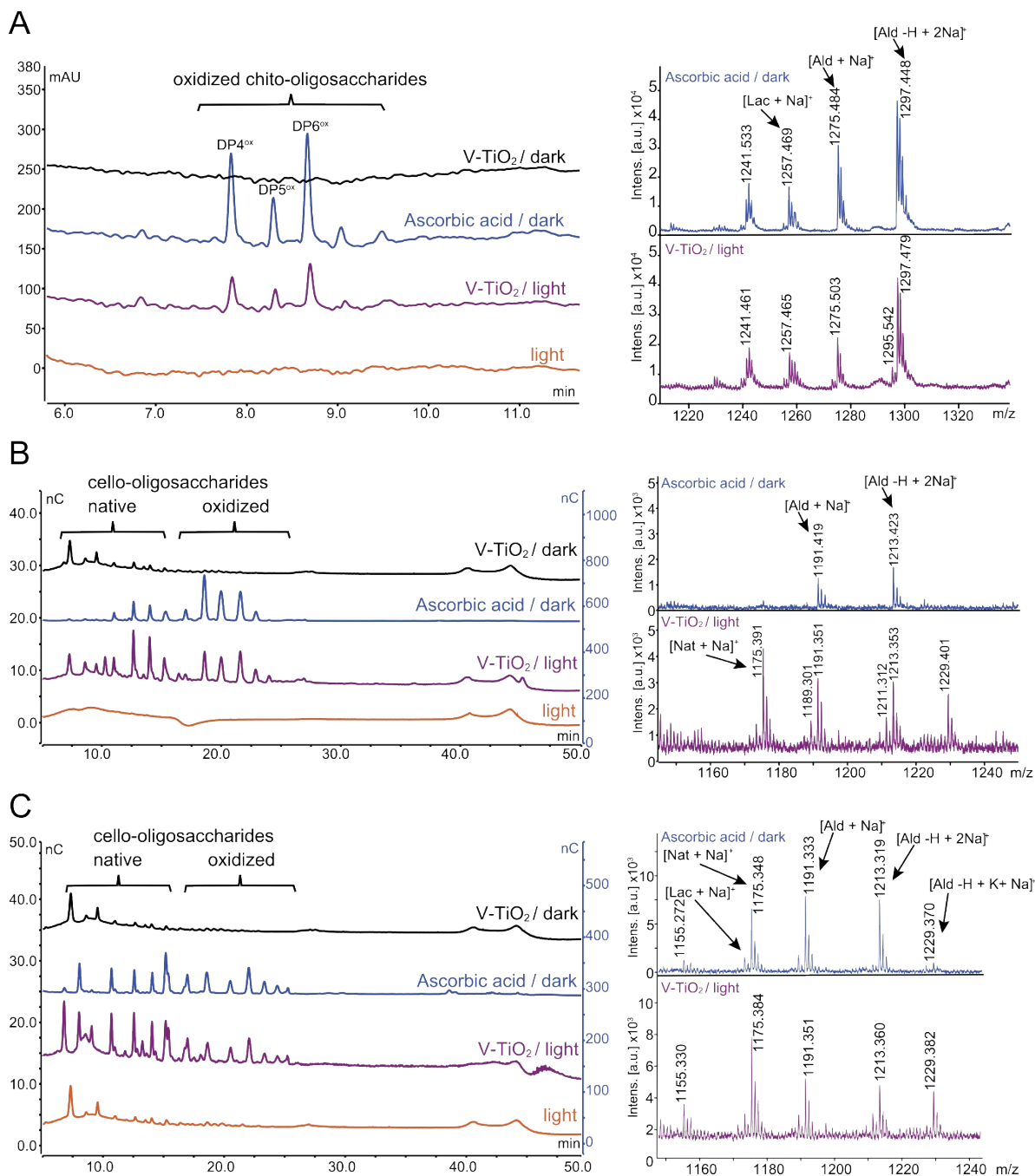


Figure S3. A substrate- and LPMO family-independent photobiocatalytic system. Product profile generated from **(A)** β -chitin (10 g.L⁻¹) by CBP21 (2 μ M), or from Avicel (10 g.L⁻¹) by **(B)** *PcLPMO9D* (2 μ M) or **(C)** *ScLPMO10B* (2 μ M). For each reaction the left panel shows chromatograms (HILIC-UV and HPAEC-PAD for chito-oligosaccharides and cello-oligosaccharides, respectively) and the right panel shows MALDI-TOF MS spectra for the DP7 cluster, showing adducts of the lactone (Lac) and the aldonic acid (Ald) form. Reactions were carried out during 20 h for CBP21 or 4 h for *PcLPMO9D* and *ScLPMO10B* in sodium phosphate buffer (50 mM, pH 6.0) at 40 °C, under magnetic stirring, with exposure to light when stated ($I=25\%I_{\max}$, approx. 42 W.cm⁻²) and addition of ascorbic acid (1 mM final concentration) when

stated. V-TiO₂ was added to a final concentration of 10 g.L⁻¹, when stated. Abbreviations: DP, degree of polymerization; Nat, native; ox, oxidized; Lac, lactone form; Ald, aldonic acid form. The LPMOs used in panel **(A)** and **(B)** are both strict C-1-oxidizers, acting on chitin and cellulose, respectively. The LPMO used in panel **(C)** can oxidize both C-1 and C-4. The levels of C-4 oxidized products detected by HPAEC-PAD are very low due to on-column product degradation, whereas MALDI-TOF MS cannot decisively discriminate between C-1 and C-4 oxidized products (e.g. Forsberg et al., 2014, Fig. S1)¹. However, C-1/C-4 oxidizing LPMOs produce relatively high levels of native oligomers, as is indeed observed in panel **(C)**. It has been shown very recently that these native products in fact are on-column generated degradation products of C4 oxidized cello-oligomers.² NB: the secondary y-axis (blue color) used in the left panels in **(B)** and **(C)** refers to the chromatogram for the reaction with ascorbic acid.

- 1 Z. Forsberg, A. K. Mackenzie, M. Sørli, Å. K. Røhr, R. Helland, A. S. Arvai, G. Vaaje-Kolstad and V. G. H. Eijsink, *Proc. Natl. Acad. Sci. U. S. A.*, 2014, **111**, 8446–8451.
- 2 B. Westereng, M. Ø. Arntzen, F. L. Aachmann, A. Várnai, V. G. Eijsink and J. W. Agger, *J. Chromatogr. A*, 2016, 46–54.

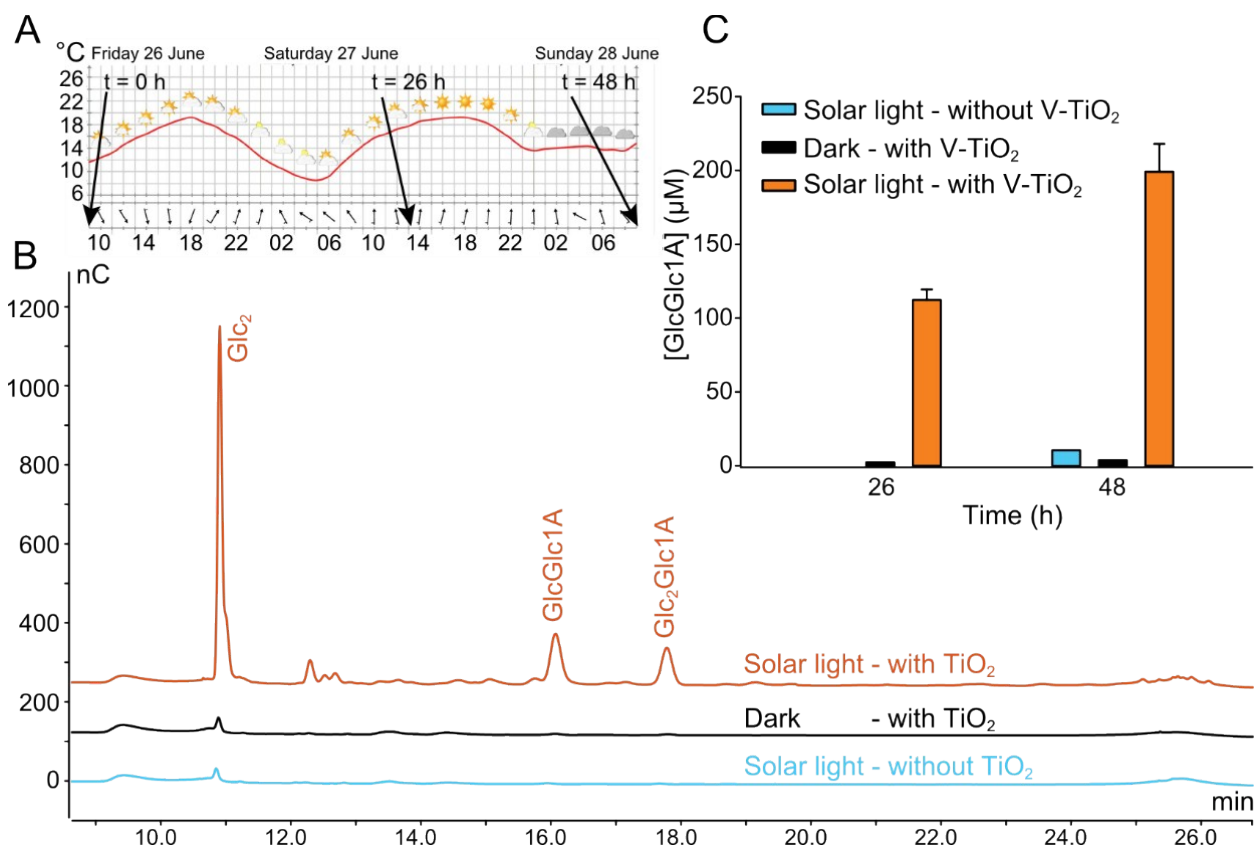


Figure S4. Harvesting sunlight energy. A reaction mixture containing V-TiO₂ (5 g.L⁻¹), ScLPMO10C (1 μM) and Avicel (10 g.L⁻¹) was exposed to sunlight through a window. **(A)** Weather forecast at NMBU (Ås, Norway) between June 26 and June 28, 2015. **(B)** HPAEC-PAD profile of oxidized products (26 h reaction time-point) after hydrolysis of LPMO-solubilized cello-oligomers by *TfCel5A* and **(C)** GlcGlc1A product quantification. Reactions were carried out in sodium phosphate (50 mM, pH 6.0), in closed glass vials under magnetic stirring (300 rpm), at approx. 30 °C. Error bars in **(C)** show ± s.d. (n = 3) for the reaction of interest containing V-TiO₂ and exposed to solar light (orange bars).

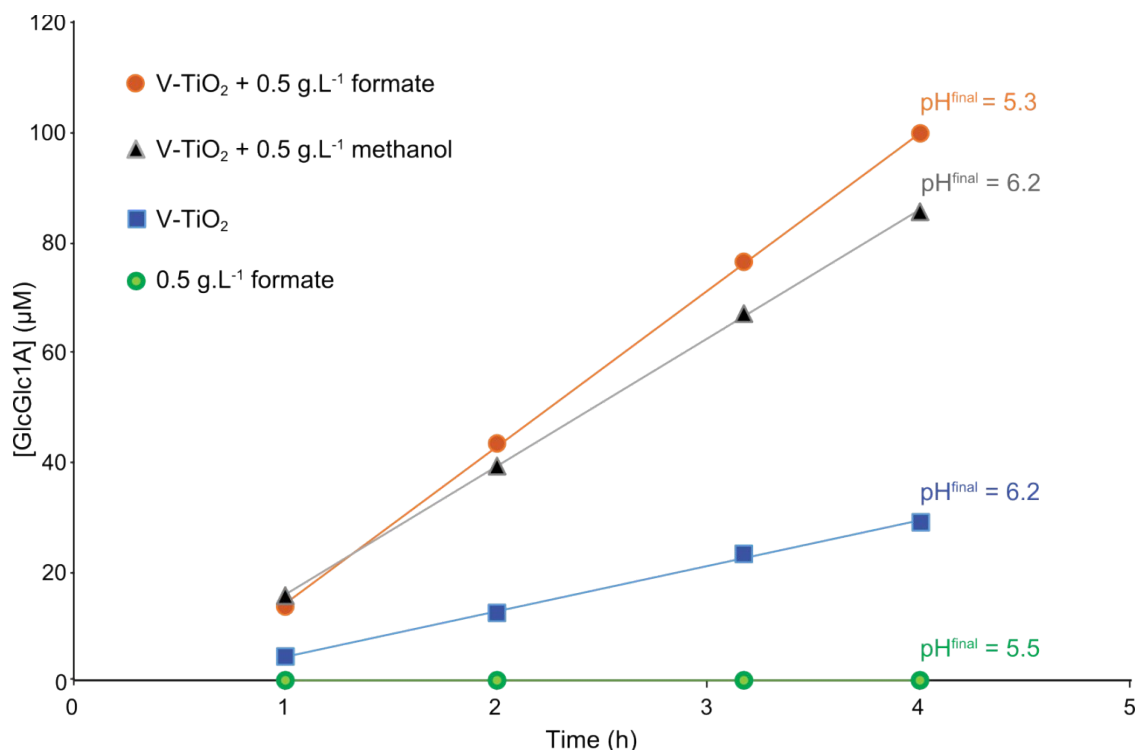


Figure S5. Impact of putative alternative electron donors (methanol or formate) on the photobiocatalytic oxidation of cellulose by ScLPMO10C. The graphs show time-courses for release of aldonic acid products by ScLPMO10C (1 μ M) from Avicel (10 g.L⁻¹) in the presence of V-TiO₂ (5 g.L⁻¹). Reactions were carried out in sodium phosphate buffer (50 mM, pH 6.0) at 40 °C under magnetic stirring with a light intensity of 25% of maximum intensity (approx. 42 W.cm⁻²) in absence or presence of 0.5 g.L⁻¹ formic acid (10.8 mM) or methanol (15.6 mM). In a control reaction (green circles) formate was added, in the absence of V-TiO₂. Before product quantification, celloligosaccharides were hydrolyzed by TjCel5A, yielding oxidized products with a degree of polymerization of 2 and 3 [GlcGlc1A, (Glc)₂Glc1A]. pH values for each reaction at t = 4 h are plotted on the graph; note that the use of formic acid had a considerable pH effect since at pH 6.0 it dissociates to formate as a main species ($pK_a = 3.75$) and lowers therefore the pH.

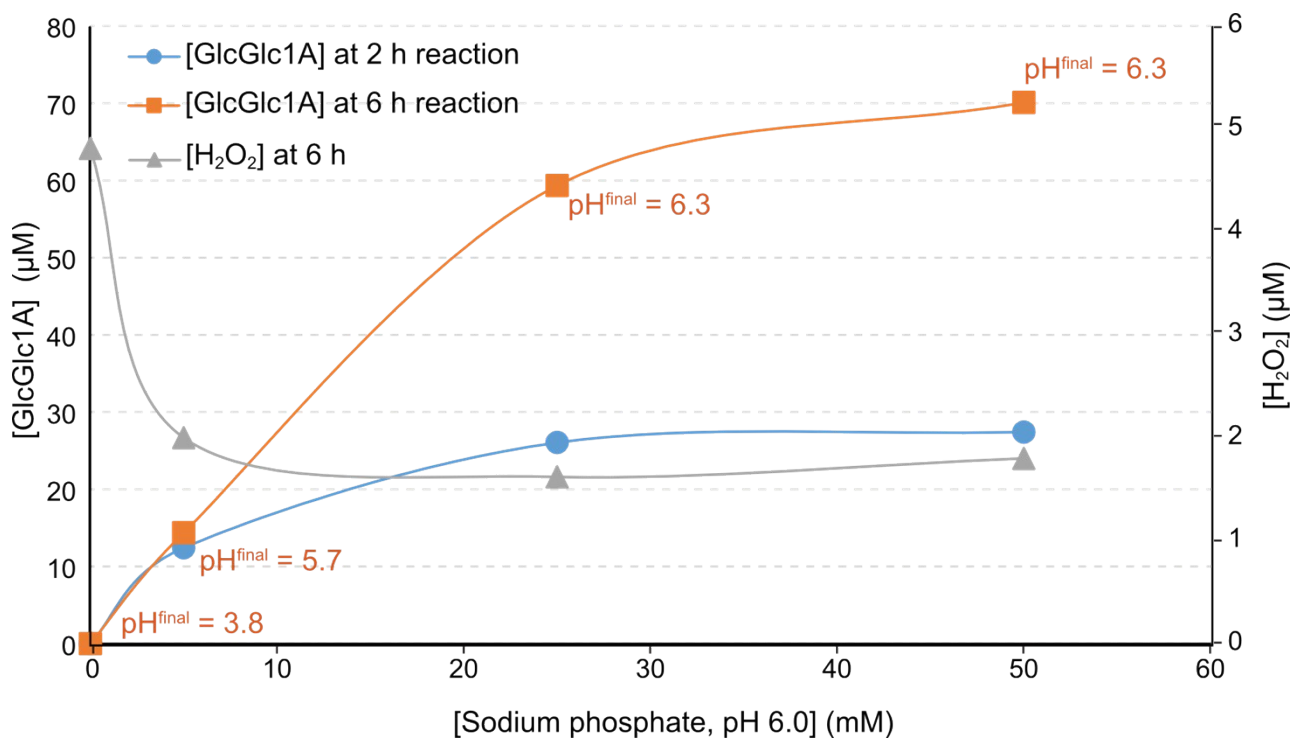


Figure S6. The effect of phosphate on the photobiocatalytic system. The figure shows dose-response curves for sodium phosphate with respect to cellulose oxidation (measured at 2 h and 6 h) and the apparent accumulation of H₂O₂, which would be produced upon oxygen reduction at the V-TiO₂ surface. All reactions were carried out with ScLPMO10C (1.5 μM) and Avicel (10 g.L⁻¹) in the presence of V-TiO₂ (5 g.L⁻¹), either in water or sodium phosphate buffer (pH 6.0) at 40 °C under magnetic stirring and under a visible light with an intensity of 25% of maximum intensity (approx. 42 W.cm⁻²). pH values were measured at the end of each reaction (t = 6 h) and are plotted on the graph. Before product quantification, celloligosaccharides were hydrolyzed by *Tf*Cel5A, yielding oxidized products with a degree of polymerization of 2 and 3 [GlcGlc1A, (Glc)₂Glc1A]. Note that the effect observed when there is no phosphate present at all is likely due in part to the pH effect. See **Fig. S7** for more data on the role of polyprotic acids.

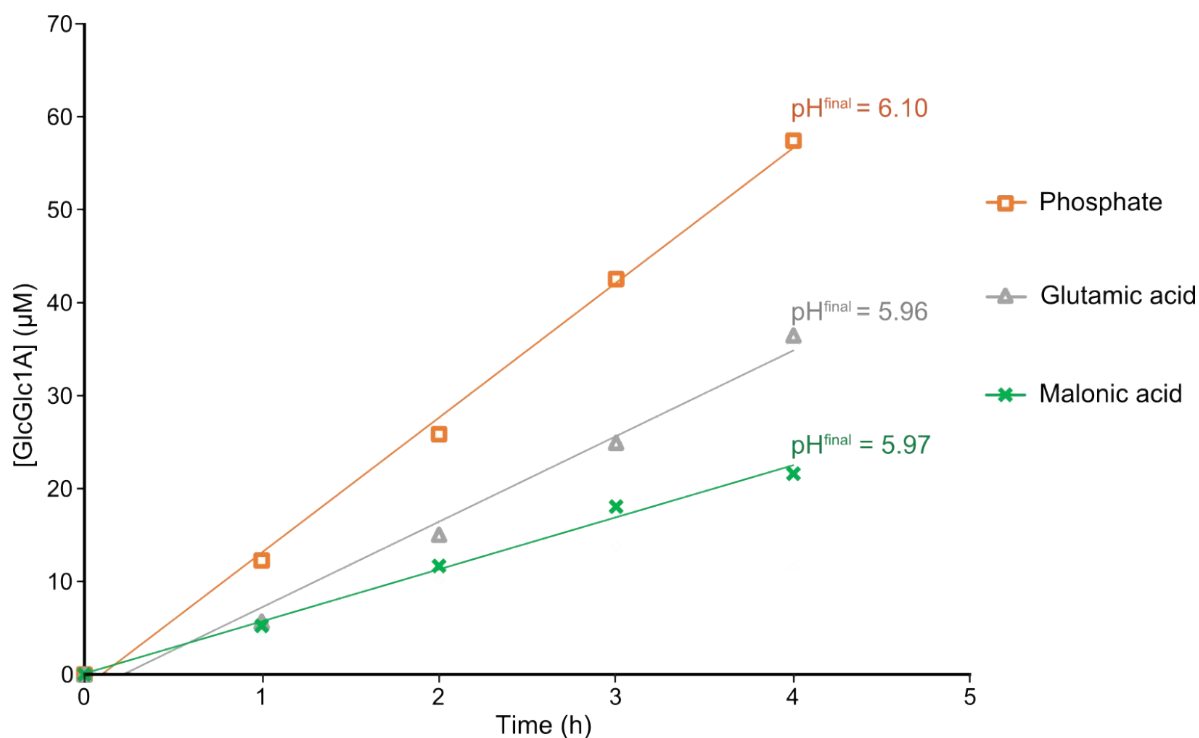


Figure S7. Role of polyprotic acids in the oxidation of Avicel by ScLPMO10C/V-TiO₂ upon visible light exposure.

The graph shows the time courses for oxidation of Avicel (10 g.L⁻¹) by ScLPMO10C (1.5 μM) in the presence of V-TiO₂ (5 g.L⁻¹). Samples were pre-incubated at 40 °C for 20 min before turning on the light. Reactions were carried out in 50 mM (pH 6.0) of sodium phosphate, glutamic acid or malonic acid buffer, at 40 °C under magnetic stirring with a visible light intensity of 25% of maximum intensity (approx. 42 W.cm⁻²). At the end of the reaction (t = 4 h) pH values were measured (plotted on the graph).

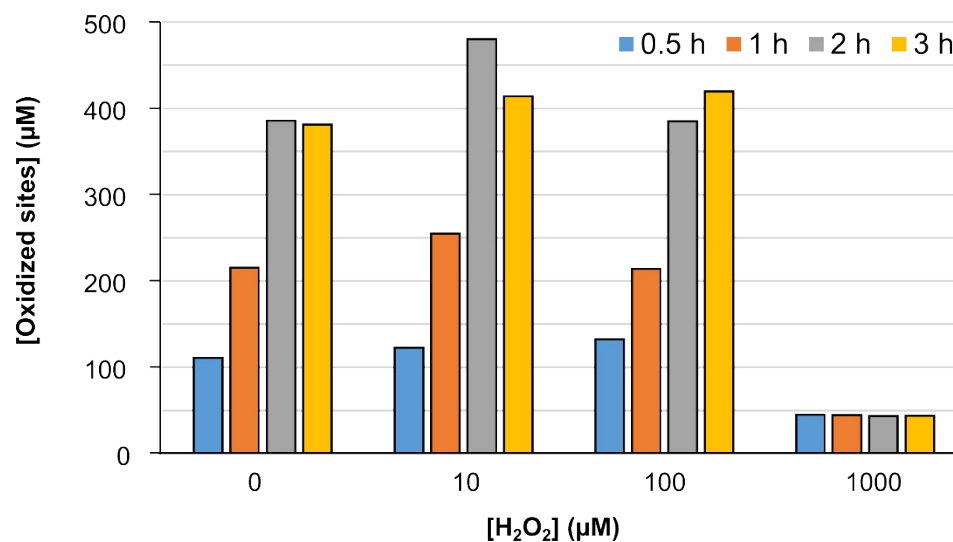


Figure S8. Impact of H₂O₂ on ScLPMO10C activity.

The graphs show time-courses for release of aldonic acid products by ScLPMO10C (0.5 μM) from Avicel (10 g.L⁻¹) in the presence of different concentrations of exogenous H₂O₂ (0 to 1000 μM). Reactions were carried out in sodium phosphate buffer (50 mM , pH 6.0) at 40 °C under magnetic stirring and were initiated by addition of ascorbic acid (1 mM). Before product quantification, celloligosaccharides were hydrolyzed by *Tf*Cel5A, yielding oxidized products with a degree of polymerization of 2 and 3 [GlcGlc1A, (Glc)₂Glc1A].

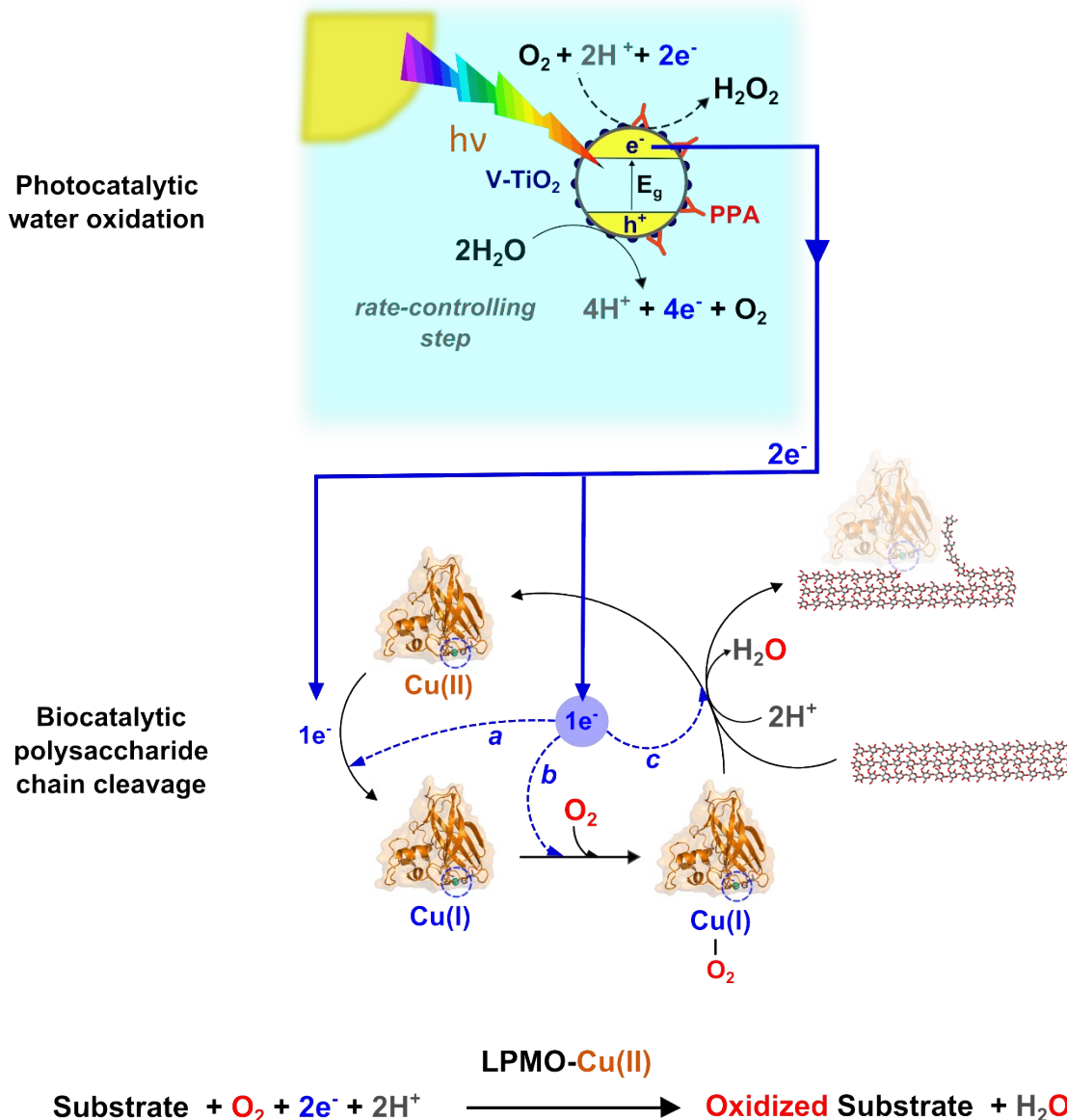


Figure S9. Schematic representation of the possible fate of electrons generated by light-driven water oxidation. Visible light is absorbed by the V-TiO₂ photocatalyst resulting in hole (h^+)-electron (e^-) pair separation and leading to O_2 production from water oxidation. In the absence of a protein electron acceptor and depending on the conditions, either e^-/h^+ recombination occurs or oxygen is reduced generating H_2O_2 or regenerating H_2O . Polyprotic acids (PPA, red “antigen”-shape) are thought to be involved in shifting O_2 reduction towards H_2O instead of H_2O_2 . We show that the generated electrons can reduce the LPMO active site copper (blue dashed circle) in the absence of a redox mediator. This initiates the LPMO catalytic cycle, leading to oxidative cleavage of polysaccharides. Two electrons are required during the overall catalytic cycle of LPMOs (cf. the global equation at bottom of figure) but the spatio-temporal features of the delivery of the second electron are still unknown. Either, this second electron can be delivered (dashed blue lines) from the very beginning (i.e. before activation of O_2 , option a), during or after binding to O_2 (option b) or through an electron channel while redox reactions

between the LPMO and the substrate are already initiated (option c). A fourth alternative (not represented on the figure) would be that the second reducing equivalent is already present within the substrate itself (e.g. trapped reduced metal ion). The orange protein structure represents the *Streptomyces coelicolor* AA10 LPMO, ScLPMO10C (PDB 4OY7). The interaction of the protein with cellulose has not been mapped experimentally and the picture is shown for illustrational purposes only. Furthermore, the chronological order of binding of the LPMO to the substrate, relatively to redox steps, is still a matter of investigations.

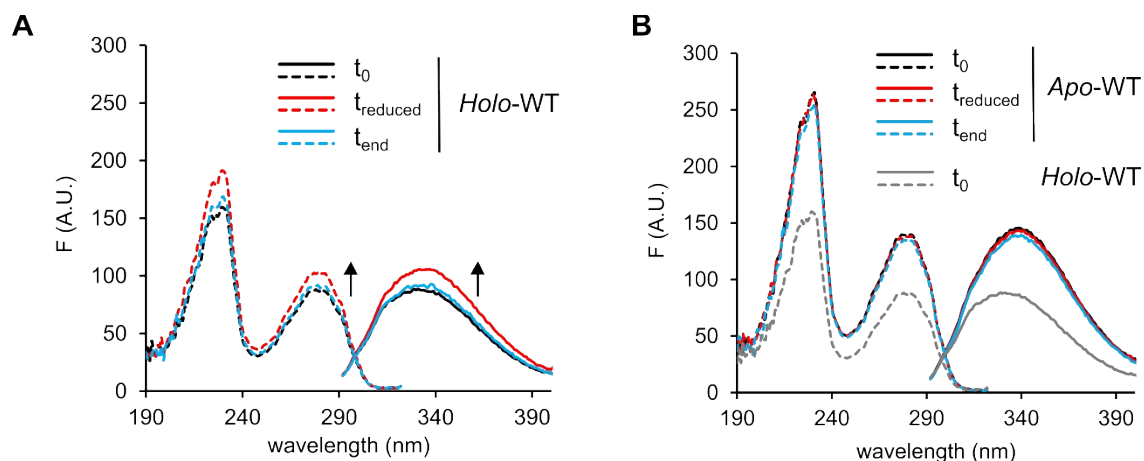


Figure S10. Redox state-dependent fluorescence properties of ScLPMO10C. The graphs show emission (excitation at 282 nm; solid lines) and excitation spectra (emission monitored at 332 nm; dotted lines) of **(A)** *holo*- and **(B)** *apo*-ScLPMO10C-WT (1 μ M) in three different states: before reduction (t_0), after reduction by ascorbic acid (t_{reduced}) and after returning to the ground state (t_{end}). In panel B, spectra for *holo*-ScLPMO10C-WT before reduction (grey line; the lower signals) are included, for comparison. In absence of copper (panel B), the absolute fluorescence of the LPMO is higher suggesting some quenching by the transition metal. Panel A shows that the magnitude of this quenching effect is dependent on the redox state the copper bound, which allowed development of the fluorescence method for monitoring reduction/oxidation (main manuscript, **Fig. 5**). The effect of the copper redox state on fluorescence quenching is likely related to modification of the electronic environment of aromatic amino acids close to the copper center.

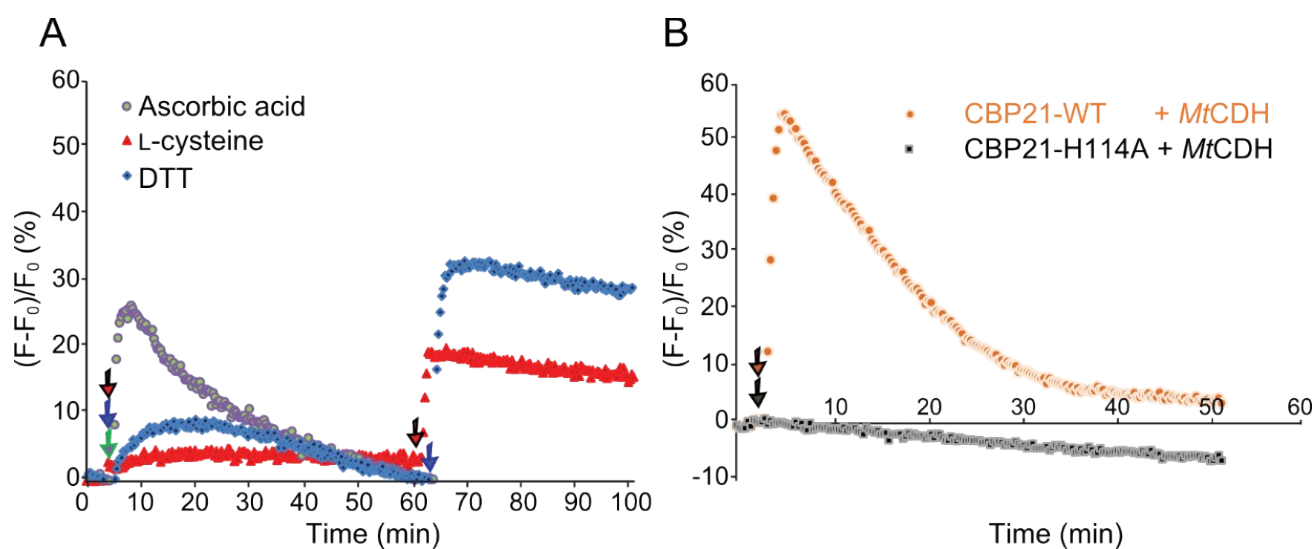


Figure S11. Probing LPMO redox intermediate formation for different redox systems by fluorescence spectrophotometry. Panel **(A)** shows the increase in fluorescence for ScLPMO10C (2 μM) upon reduction by ascorbic acid (2 μM, green arrow), L-cysteine (2 and 100 μM, added at t = 5 and t = 60 min, respectively; red arrows) or DTT (2 and 1000 μM, added at t = 5 and t = 63 min, respectively; blue arrows). Panel **(B)** shows the increase in fluorescence of CBP21 (2 μM) upon reduction by MtCDH (0.25 μM) when lactose (1 mM) was added (orange arrow); a similar experiment with the inactive H114A mutant (black arrow) did not show any increase in fluorescence. CBP21 was chosen as an LPMO model for this particular experiment since it displays a greater increase in fluorescence upon reduction, offering a better signal resolution, which is necessary due to the presence of another protein (i.e. MtCDH) with significant fluorescence background. All reactions were performed at room temperature, under stirring, in sodium phosphate buffer (pH 6.0, 50 mM).

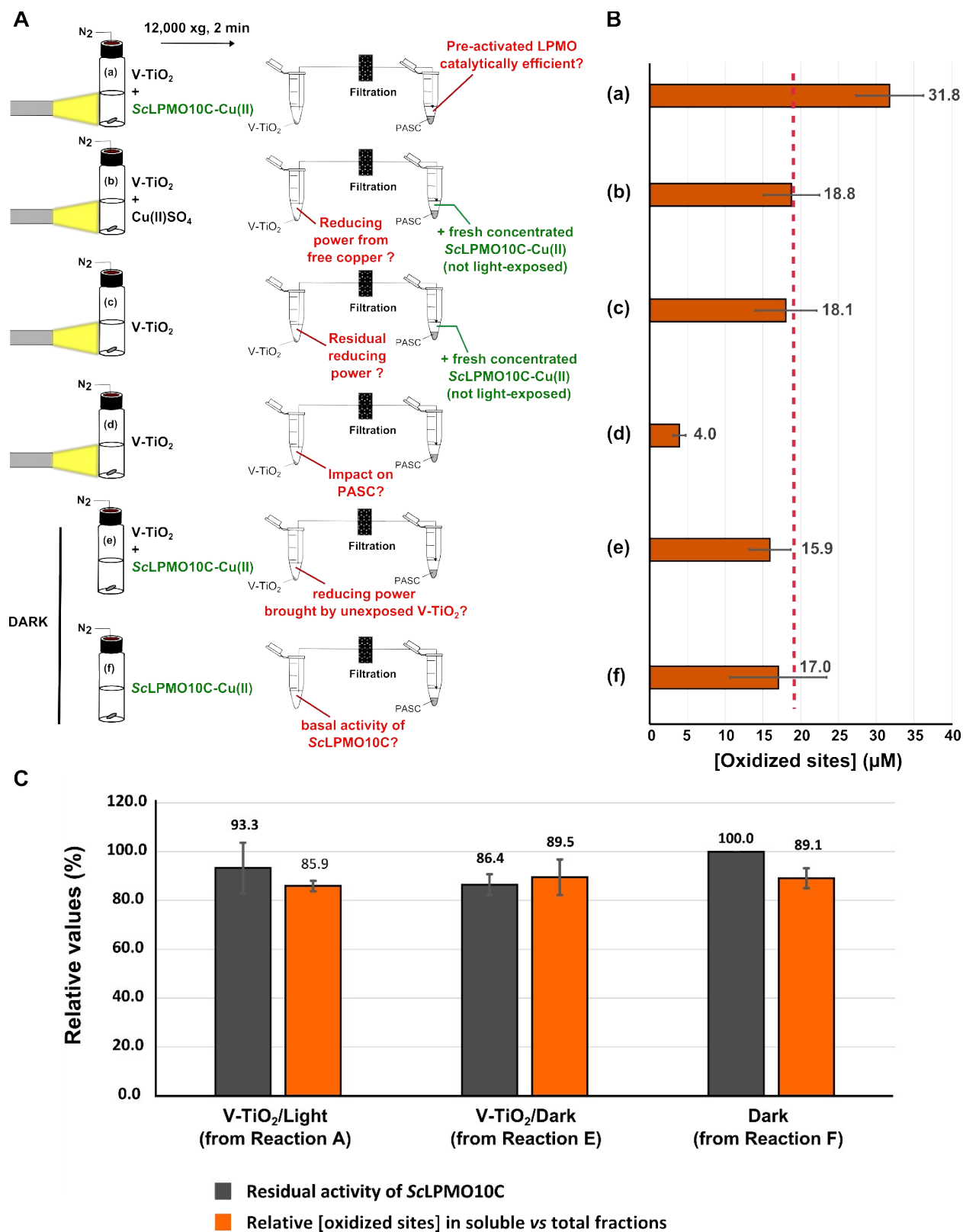


Figure S12. Shedding light on the spatio-temporal origin of electrons in the catalytic mechanism of LPMOs using the photobiocatalytic system. This figure and its legend provide a detailed explanation of

the experiments shown in **Figure 5C** (= panel B of this figure) of the main manuscript. **(A)** Experimental set up to test pre-activation of the LPMO. Prior to light exposure, all the reaction were flushed with nitrogen in order to minimize re-oxidation of the copper center by oxygen (the same protocol was followed for “dark” reactions). A reaction containing ScLPMO10C (14 μM) and V-TiO₂ (5 g.L⁻¹) was exposed to light in order to reduce ScLPMO10C-Cu(II) to ScLPMO10C-Cu(I) (**reaction a**). Control reactions containing free Cu(II)SO₄ (5 μM) or only sodium phosphate with V-TiO₂ (5 g.L⁻¹) were also prepared (**reactions b and c**). Control reactions containing ScLPMO10C (14 μM), with or without V-TiO₂ (5 g.L⁻¹) incubated in the dark were also conducted (**reactions e and f**). After 2 hours exposure to visible light ($I=25\%I_{\text{max}}$, approx. 42 W.cm⁻²) or storage in the dark, the reaction mixtures were centrifuged and the resulting supernatants were subsequently filtered to separate the electron source from the LPMO. The filtrate (100 μL) was then added to a PASC suspension (100 μL , 0.56% w/v). For reactions (b) and (c) that did not contain enzyme during the pre-activation phase, fresh unexposed ScLPMO10C-Cu(II) (to a final concentration of 7 μM) was added to the PASC solution to probe the reducing power in the filtrate. The filtrate from **reaction (d)**, which was identical to reaction (c), was added to PASC without addition of enzyme to check whether the V-TiO₂ light-exposure had generated compounds that could oxidize PASC. The reactions with PASC were incubated in a thermomixer (40 °C, 1000 rpm) during 24 h, in the dark. Five identical PASC suspensions (0.28 % w/v) in sodium phosphate buffer (50 mM, pH 6.0) were incubated at 40 °C, 1000 rpm, for 24 h as controls, to determine the background of oxidized products. All samples, including the PASC-only controls, were thermally treated (98 °C, 15 min) to inactivate the LPMO and the reaction mixtures were then hydrolyzed by a mixture of cellulases, *TfCel5A* and *TrCel7A*, to allow quantification of oxidation sites by HPAEC-PAD.

(B) Quantification of oxidized products generated in the reactions displayed in panel A. The number of oxidized sites was calculated from the quantification of GlcGlc1A and (Glc)₂Glc1A. Glc1A was excluded from calculations since it was minor and unreliable due to overlapping signals representing other compounds. The background of oxidized sites present in the PASC (83 \pm 5 μM) was subtracted from all values displayed. Note that the amounts of newly generated oxidation sites, expectedly, are low and, for reaction (d) only, not significantly above background. This panel also appears in the main manuscript, as **Figure 5C**.

(C) Activity control of ScLPMO10C exposed to light/TiO₂, dark/V-TiO₂ or dark only. From the filtrate of reactions (a),(e) and (f) an activity test on PASC was performed using ascorbic acid as a reducing agent (1 mM) to ensure that the amount of catalytically competent enzyme was similar in all reactions (and therefore comparable). These reactions were incubated at 40 °C, 1000 rpm, for 24 h followed by inactivation of the LPMO. Hydrolysis of the reaction mixture was then carried out by a mixture cellulases, *TfCel5A* and *TrCel7A*, either on the soluble fraction or on the total fraction, to allow quantification of GlcGlc1A and (Glc)₂Glc1A. The graphs represent relative activities compared to the one measured for unexposed ScLPMO10C (dark condition, reaction f; 100 % = 715 \pm 11 μM of GlcGlc1A + (Glc)₂Glc1A). The amount of oxidized products found in the soluble fraction relative to the amount found in the total fraction is also represented, showing that approx. 10% of oxidized products was trapped in the insoluble fraction.